

Figure 1. Power loss density distribution at 60 GHz (a) sweat gland; (b) nerves; (c) blood vessels; (d) pilosebaceous unit; (e) Meissner corpuscle; (f) lymphatic vessels; (g) Pacinian corpuscle.

S09-6 [11:15]
STUDENT PAPER

Novel procedure for spatial averaging of absorbed power density on realistic body models at millimeter waves

Ante Lojic Kapetanovic¹, Giulia Sacco², Dragan Poljak¹ & Maxim Zhadobov²

¹*Department of Electronics and Computing, University of Split, Split, Croatia, 21000*

²*IETR - UMR 6164, University of Rennes 1, CNRS, Rennes, France, 35000*

Keywords: *Dosimetry (computational), RF/Microwaves, Completed (unpublished)*

Presented by: *Ante Lojic Kapetanovic*

In this work, we propose a novel procedure for the spatial averaging of the absorbed power density (APD) on complex conformal anatomical models, which is a crucial step in the advancement of accurate dosimetry. To validate our method, the electromagnetic (EM) dosimetric analysis is performed for an ear model exposed to a plane wave at 60 GHz. We investigate the influence of two factors on the spatial-average APD: (i) the shape of the averaging surface (square and disk), and (ii) the polarization of the incident field. According to analyzed exposure scenarios, the spatial-average APD variations as a function of the averaging surface shape are less significant (tenfold) than those related to the polarization of the incident field.

1 Introduction

Millimeter wave (mmW) spectrum is a promising solution for new and emerging wireless technologies (5G, IoT, human-centered communications, etc.) due to the large available bandwidth and high data rates [1]. Even though the radiation at mmW is nonionizing, widespread use of personal and on-body devices operating at such frequencies is causing increased public concern with regards to biological safety [2]. International guidelines [3] and IEEE standards [4] for human exposure to EM fields have recently been revised, and the absorbed (epithelial) power density spatially averaged across an irradiated surface of the tissue is defined as the basic restriction (dosimetric reference limit) at frequencies above 6 GHz. Below 30 GHz, the APD should be averaged over a $2 \times 2 \text{ cm}^2$ surface to account for the consistency with the volume average basic restriction at lower frequencies, and to provide close approximation to local maximum temperature rise [5]. Between 30 GHz and 300 GHz, the APD should additionally be averaged over a $1 \times 1 \text{ cm}^2$ surface and should not exceed 2 times the value for the $2 \times 2 \text{ cm}^2$ surface. The state-of-the-art assessment of the spatial-average APD (APD_{av}) uses planar tissue models [6]. Some efforts have been made to compute the APD_{av} and temperature rise on non-planar body models [7] where canonical structures with a diameter equal or longer than the side of the square surface for averaging is considered at and above 6 GHz.

In this paper, we tackle the problem of accurate evaluation of the APD_{av} over a realistic surface at mmW, which, to the best of our knowledge, has never been addressed so far. We propose a technique that handles conformal averaging of the APD seamlessly regardless of geometrical complexity of the considered surface. The impact of the shape of the averaging surface, as well as the polarization of incident fields, is analyzed and set in the context of the current guidelines/standards.

2 Materials and Methods

2.1 Electromagnetic Model

A morphologically-accurate ear model, shown in Fig. 1(a), has been considered for the EM exposure analysis. Dimensions are chosen to match the average ear length (54.97 mm) and width (35.41 mm) for a middle-age adult [8]. The complex permittivity of the model is set to $7.98 - j10.90$ to match the value of the adult dry skin [9]. Prior to simulation, the model is discretized by utilizing a tetrahedral mesh with the maximal size of a mesh cell set to $\lambda/8$ resulting in about 15 million mesh cells overall. A plane wave, impinging the helix of the model (z-axis direction), is

defined as a source of EM radiation at 60 GHz. The analysis is performed for transverse electric (TE) and transverse magnetic (TM) polarization. The EM field distribution in the model is computed with the frequency domain solver available in CST Studio Suite by means of the finite element method (FEM) with perfectly matched layers imposed in all directions to emulate the open space exposure conditions.

2.2 Assessment of Spatial-Average Absorbed Power Density

Power density on the surface of the model is defined as the time-average Poynting vector:

$$\mathbf{P} = \frac{1}{2} \Re[\mathbf{E} \times \mathbf{H}^*] \quad (\text{Eq.1})$$

where \mathbf{E} and \mathbf{H} are complex phasor electric and magnetic fields, respectively, and $*$ is the complex conjugate operator. The APD is defined as the normal component of \mathbf{P} on the oriented surface:

$$APD = \mathbf{P} \cdot \mathbf{n} \quad (\text{Eq.2})$$

where \mathbf{n} is the unit normal vector field over the surface. The spatial distribution of the APD is visualized in Fig. 1(b) and Fig. 1(c) for TE and TM polarization, respectively.

The unit vector field normal to the model's surface is estimated at the same points in which the APD is computed. For each point, a normal vector is assigned by fitting a local hyperplane that minimizes the sum of square distances from the local neighborhood of a point. The first step is to find a local neighborhood, in this case, via k-nearest neighbors algorithm with a predefined number of neighboring points, k , set to 100. Principal component analysis (PCA) regression is used to find an orthogonal basis by computing the eigenvectors and eigenvalues of a covariance matrix created from the local neighborhood of a query point [10]. The normal vector is then defined as the eigenvector with the smallest eigenvalue. Since the PCA arbitrarily orients eigenvectors, the normal vector field is not consistently oriented across the surface. The second step is to build a graph connecting adjacent points of the model [10], again by using the k-nearest neighbors algorithm with k set to 30. The normal vector orientation is propagated starting from a desired viewpoint, in this case, with respect to positive z-axis direction to match the plane wave incidence. The spatial distribution of the unit normal vector field across the surface of the model is shown in Fig. 1(d).

The APD_{av} is defined as the spatial average of the APD over the averaging surface of area A [3]:

$$APD_{av} = \frac{1}{A} \iint_A APD \, dA \quad (Eq.3)$$

The surface integral in Eq. (3) is approximated as a weighted sum of incremental contributions of the APD across A. Schematic overview of the integration process over a square-shaped averaging surface is visualized in Fig. 2 for the case of TE polarization. The 2-dimensional Gaussian-Legendre quadrature is utilized for a square-shaped integration domain where the nodes are selected as roots of the 6th degree Legendre polynomials, and weights are derived for each corresponding node [11]. The 12th degree symmetric quadrature formula for a unit disk [12] is used for a disk-shaped integration domain. Both quadrature techniques yield exactly 36 nodes, thus reaching the same level of spatial and computational complexity.

3 Results and Discussion

The analysis on the influence of the averaging surface shape and polarization on the maximal APD_{av} is performed. In addition to the prescribed square of 1 cm², we consider a disk with a radius of 0.56 cm (to match the 1 cm² area). Both averaging surfaces are centered around the middle point of the most irradiated region of the helix which results with the maximal APD_{av} . The spatial distribution of the APD is shown in Fig. 3(a) for TE and in Fig. 3(d) for TM polarization. The APD across a square- and disk-shaped averaging surface is respectively represented in Fig. 3(b) and in Fig. 3(c) for TE polarization, while Fig. 3(e) and Fig. 3(f) correspond to TM polarization. The incident power density of 10 Wm⁻² results in a maximal APD_{av} of 5.73 Wm⁻² averaged over a disk-shaped surface for a TE polarized plane wave, while a minimal value is 4.80 Wm⁻² for a TM polarized plane wave and a square-shaped averaging surface. The main results are summarized in Table 1.

Table 1. Main results of the analysis.

APD _{av} [Wm ⁻²]		averaging surface shape		relative difference [%]
		square	disk	
polarization	TE	5.61	5.73	1.81
	TM	4.80	4.85	0.92
relative difference [%]		13.11	14	

By considering the APD_{av} of 6.22 Wm⁻² averaged across square 1 cm² surface of a planar homogeneous

model illuminated by a plane wave with a normal incidence as a reference value, the relative difference of the APD_{av} between a square- and a disk-shaped surface is 1.81 % and 0.92 % for TE and TM polarization, respectively. The relative difference between TE and TM polarization results in 13.11 % and 14 % for a square- and a disk-shaped surface, respectively. This indicates that APD_{av} variations as a function of the averaging surface geometry are marginal (within 2 %). However, the polarization of the incident field significantly affects the APD_{av}, according to studied exposure scenarios.

4 Conclusion

We propose a novel procedure for spatial averaging of the APD over non-planar surfaces on a tissue-equivalent model. The proposed method achieves two improvements over a conventional approach: assessment of the APD_{av} on realistic models, and employment of accurate quadrature techniques for arbitrarily shaped averaging surfaces. We present the analysis of the EM exposure of a realistic ear model illuminated by a plane wave at 60 GHz. The EM field distribution across the surface of the model is computed by FEM implemented in the commercial software (CST), while the unit vector field normal to the model's surface is estimated by the PCA regression. The spatial averaging is defined as the surface integral of the normal component of the APD over the oriented surface. Two sets of variables have been considered: (i) averaging surface geometries, and (ii) the polarization of incident fields. The results indicate that variations of the APD_{av} influenced by surface geometry are marginal, while the polarization of incident fields carry substantial impact. The findings demonstrate promising potential of the proposed method for retrieval of mmW dosimetric quantities on complex conformal anatomical models, which is of uppermost importance for accurate dosimetry.

Acknowledgments

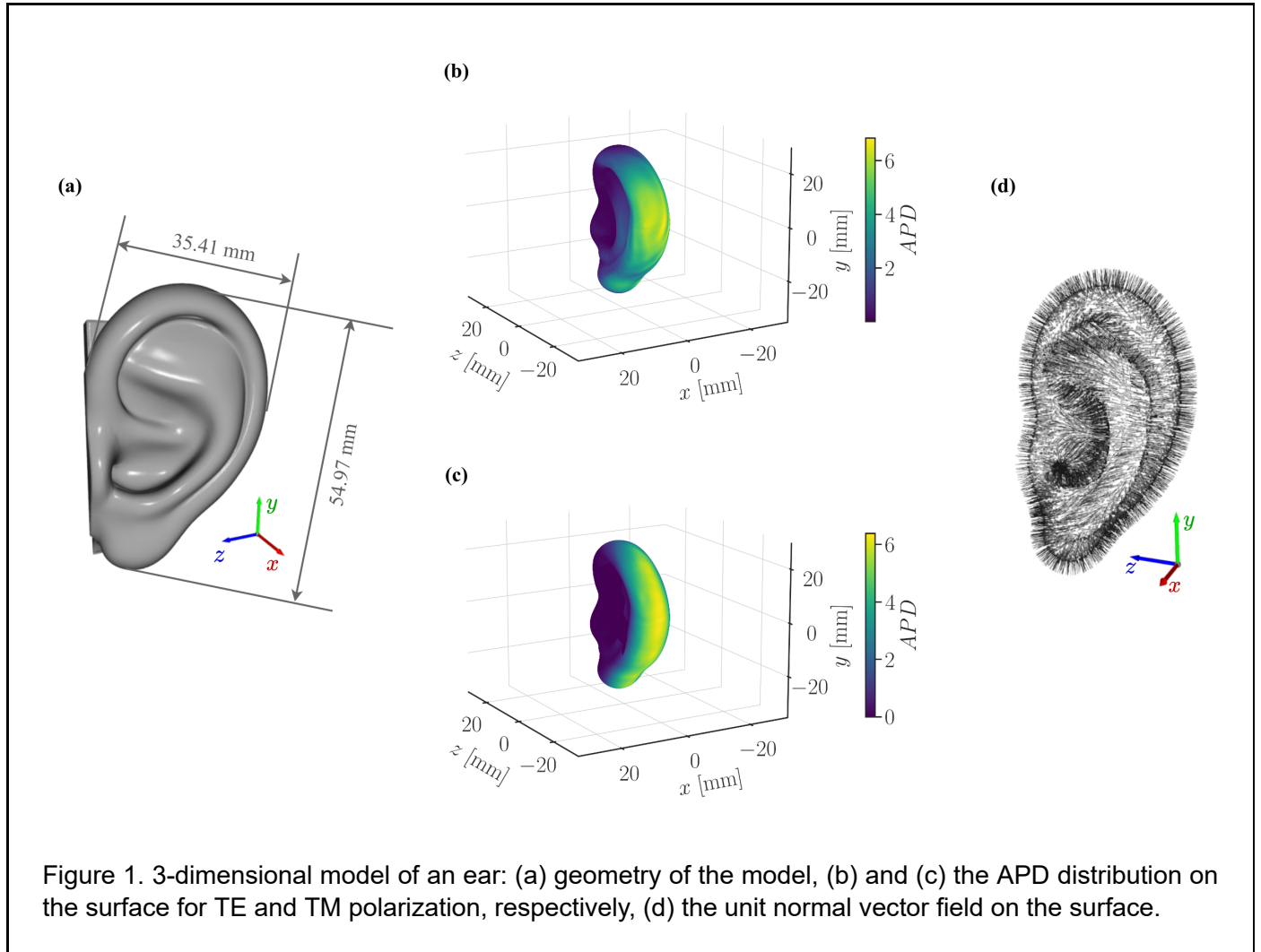
This research has been supported by the European Regional Development Fund under the grant KK.01.1.1.01.0009 (DATACROSS), the French National Research Program for Environmental and Occupational Health of ANSES under Grant 2018/2 RF/07 through the NEAR 5G Project, and has also received funding from the European Union's Horizon 2020 research and innovation programme under the Marie Skłodowska-Curie grant agreement N° 899546.

References

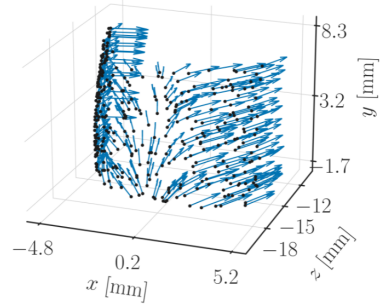
- [1] M. Zhadobov, N. Chahat, R. Sauleau, C. Le Quement, and Y. Le Drean. Millimeter-wave interactions with the human body: state of knowledge and recent advances. *International Journal of Microwave and Wireless Technologies*, 3(2):237–247, 2011.
- [2] T. Wu, T. S. Rappaport, and C. M. Collins. Safe for generations to come: Considerations of safety for millimeter waves in wireless communications. *IEEE Microwave Magazine*, 16(2):65–84, 2015.
- [3] ICNIRP. Guidelines for limiting exposure to electromagnetic fields (100 kHz to 300 GHz). *Health Physics*, 118:483–524, 2020.
- [4] IEEE standard for safety levels with respect to human exposure to electric, magnetic, and electromagnetic fields, 0 Hz to 300 GHz. IEEE Std C95.1-2019 (Revision of IEEE Std C95.1-2005/Incorporates IEEE Std C95.1-2019/Cor1-2019), pages 1–312, 2019.
- [5] Y. Hashimoto, A. Hirata, R. Morimoto, S. Aonuma, I. Laakso, K. Jokela, and K. R. Foster. On the averaging area for incident power density for human exposure limits at frequencies over 6 GHz. *Physics in Medicine and Biology*, 62(8):3124–3138, 2017.
- [6] A. Hirata, S. Kodera, K. Sasaki, J. Gomez-Tames, I. Laakso, A. Wood, S. Watanabe, and K. R. Foster. Human exposure to radiofrequency energy above 6 GHz: review of computational dosimetry studies. *Physics in medicine & biology*, 66(8):08TR01, 2021.
- [7] Y. Diao, E. A. Rashed, and A. Hirata. Assessment of absorbed power density and temperature rise for nonplanar body model under electromagnetic exposure above 6 GHz. *Physics in medicine & biology*, 65(22):224001, 2020.
- [8] C. Sforza, G. Grandi, M. Binelli, D. G. Tommasi, R. Rosati, and V.F Ferrario. Age- and sex-related changes in the normal human ear. *Forensic Science International*, 187(1):110.e1–110.e7, 2009.
- [9] C. Gabriel. Compilation of the dielectric properties of body tissues at RF and microwave frequencies. US Air Force, Final Technical Report:TR-1996-0037, 1996.

- [10] H. Hoppe, T. DeRose, T. Duchamp, J. McDonald, and W. Stuetzle. Surface reconstruction from unorganized points. ACM Special Interest Group on Computer Graphics, 26(2):71–78, 1992.
- [11] M. Abramowitz and I. A. Stegun. Handbook of Mathematical Functions With Formulas, Graphs, and Mathematical Tables, chapter 25.4.29. Dover Publication, 1972.
- [12] K. Kim and M. Song. Symmetric quadrature formulas over a unit disk. Korean Journal of Computational & Applied Mathematics, 4:179–192, 1997.

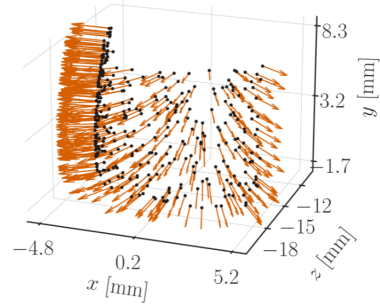
Figures



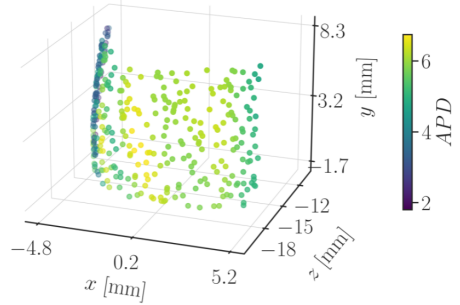
(a)



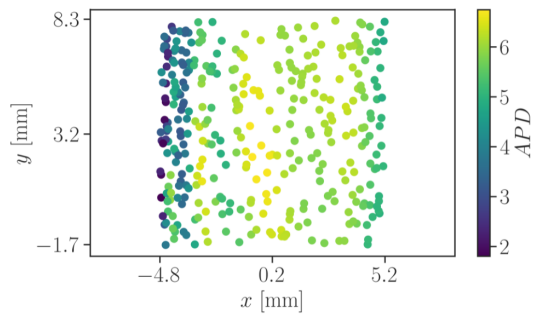
(b)



(c)



(d)



(e)

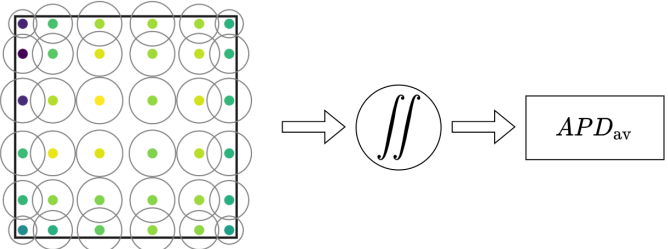


Figure 2. Spatial averaging of the APD across square-shaped surface for the case of TE polarization: (a) the time-average Poynting vector, (b) the unit normal vector field, (c) the APD as a result of a scalar product between vector fields shown in (a) and (b), (d) the APD scalar field mapped to a 2-dimensional parametrized surface for spatial averaging, (d) the distribution of the integration nodes (colored points) and weights (radii of each small circle surrounding integration node), with the final APD_{av} . The total number of points in (a), (b), (c) and (d) is uniformly downscaled by a factor of 20 for visualization sake

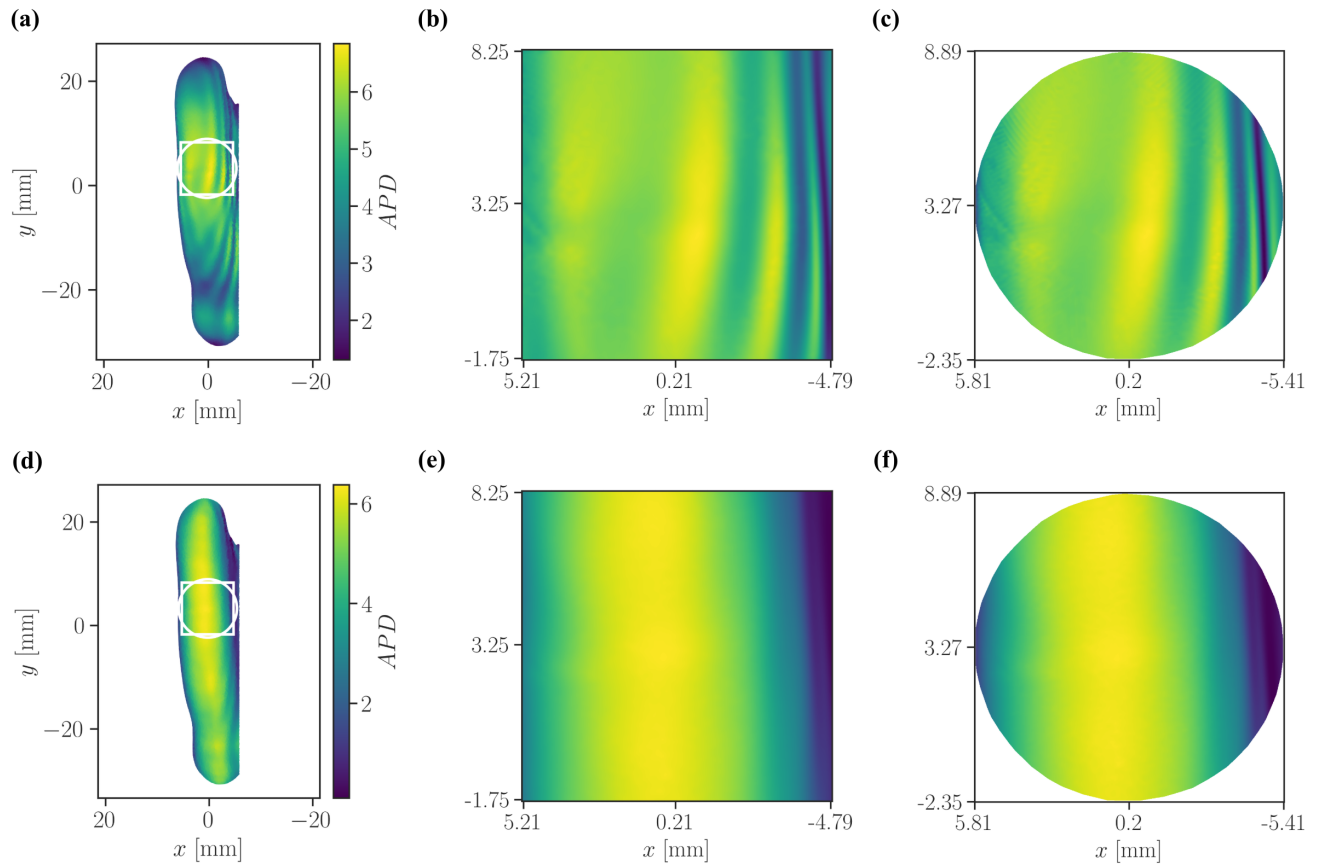


Figure 3. Square- and disk-shaped domains are used for the assessment of the APD_{av} . (a), (b), and (c) correspond to TE polarization, while (d), (e), and (f) correspond to TM polarization. Columns respectively show the most exposed surface, the square-shaped averaging surface and the disk-shaped averaging surface of the model.